

# Small-scale superadiabatic combustors with a two-step chain-branching chemistry model: asymptotic models and the effect of two-dimensionality on lean mixtures burning

Javier Bosch, Daniel Fernández-Galisteo, Carmen Jiménez, Vadim N. Kurdyumov\*

*Department of Energy, CIEMAT, Avda. Complutense 22, 28040 Madrid, Spain*

---

## Abstract

Small-sized super-adiabatic combustion devices consisting of countercurrent channels with heat-exchange segments are investigated for their ability to burn ultra-lean mixtures. The study is carried out numerically using a two-step chain-branching kinetic model in which the flammability limit appears explicitly. Various asymptotic approximations for modeling the process are considered, together with the solution of the two-dimensional conservation equations for species and temperature in the gas and the solid walls. The influence of the width of the channels and the separating walls properties on the efficiency of the device in burning mixtures below the flammability limit is investigated. The main goal of the study is to determine the applicability of the considered asymptotic models for the effective prediction of the operation of such combustion devices.

*Key words:* Micro combustion, Narrow-channel approximation, Laminar premixed flame, Two-step kinetic model, Intermediate chain-branching chemistry

---

\*Fax: +34 91 346 6269.

*Email address:* [vadim.k@ciemat.es](mailto:vadim.k@ciemat.es) (Vadim N. Kurdyumov)

## Novelty and significance statement

In this work, the appearance of non-symmetric structures for diffusion combustion is investigated for the first time within the framework of the coupled Navier-Stokes and transport equations. In the considered configuration fuel and oxidizer are injected from a porous plug into a planar channel forming two edge flames. The simultaneous appearance of symmetrically and non-symmetrically situated edge flames is demonstrated, and the regions of existence of such structures are investigated.

## Authors contributions

JB - performed research, wrote the paper; DFG - performed research, wrote the paper; CJ - performed research, wrote the paper; VNK - performed research, wrote the paper.

## 1. Introduction

Understanding and ensuring ultra-lean burning is an important issue in combustion science, as a fundamental scientific problem, and also in view of its practical application as a clean combustion technology for power generation from renewable hydrogen, for example. Ensuring ultra-lean combustion refers here to designing devices that can provide self-sustained combustion under the lean flammability limit. Although the concept of a flammability limit has received widespread attention due to its importance in safety matters, and the combustion literature provides numerous data on the corresponding concentrations of combustible substances based on experimental studies, a rigorous mathematical definition of this concept lacks clarity in the general case. A refinement of this concept can be made relating the definition to the existence of a planar combustion front, at least as a mathematical object<sup>1</sup>, obtained for a given kinetics under the idealized conditions of the absence of heat losses. In fact, this is the same definition found in a classical combustion text book, which is: "flammability limits are limits of composition or pressure beyond which a fuel-oxidizer mixture cannot be made to burn", see [1] (p. 266 in chapter 8).

---

<sup>1</sup>Planar flame fronts can be unstable.

In a mathematical sense, the flammability limit can be also associated with the existence of a crossover temperature. Namely, if the temperature reached after complete burning of all the available fuel at a constant pressure <sup>2</sup> (in other words, the mixture adiabatic temperature) is below this crossover temperature, then there is no solution in the form of a planar flame front. Obviously, this is a chemical-kinetic definition of the flammability limit that cannot be applied to every kinetic scheme. For example, this is not applicable to the simple one-step kinetics of the Arrhenius type, since within the framework of this combustion model a planar combustion wave solution always can be found (in the absence of heat loss, of course), and there is no restriction on the concentration of the combustible substance. Within this model no crossover temperature exists.

Perhaps the simplest chemistry model in which the flammability limit is clearly presented is the two-step kinetics scheme proposed in [3, 4, 5, 6]. This chain branching chemistry scheme is a modification of the kinetics proposed by Zel'dovich [7, 8, 9]. It was referred by Zel'dovich as an idealized case of the hydrogen-oxygen combustion [8]. This mechanism was explored later by Liñán [10] using the high activation energy asymptotic (HAEA) limit where fast, intermediate and slow recombination regimes were identified. Sometimes this model is referred in the literature as the Zeldovich-Liñán (ZL) model. The HAEA analysis was carried out in [11] where non-zero heat release was assumed also for the autocatalytic step. The effect of this kinetic scheme on the properties of the combustion wave has been reported in various publications. The asymptotic structure of the front was considered in [12], the linear stability results were reported in [13, 14, 15, 16, 17, 18] together with other features of the propagating wave in [19, 20].

The existence of a crossover temperature was demonstrated in [21, 22, 23] for a reduced kinetics for lean hydrogen-air deflagrations. The reduced kinetics was a non-Arrhenius one-step kinetics and allowed the definition of a crossover temperature. Interestingly, when using a complete kinetic mechanism for hydrogen, such as that proposed in [24], a crossover temperature cannot be detected and, apparently, a planar deflagration front exists for any arbitrarily low hydrogen concentration [25, 26]. It seems that reactions involving H<sub>2</sub>O<sub>2</sub>, which are not included in the reduced one-step kinetics de-

---

<sup>2</sup>The combustion temperature at constant volume can be higher than that at constant pressure [2].

veloped in [21, 22, 23], activate a slow path of hydrogen oxidation. This path, which is extinguished under small radiant heat loss, is also negligible for describing planar deflagrations at high temperature, enabling a one-step reduced kinetic description. A detailed overview of these problems and their applications, along with a detailed discussion, can be found in [27].

A canonical design of a superadiabatic burner consists of two or more heat-exchanging parallel channels through which the combustible mixture is fed in alternating opposite directions. The underlying idea of this sort of devices based on heat recirculation should be traced back to [28, 29, 30]. This heat recirculation configuration leads to preheating of the mixture in the adjacent channel by hot products. As a consequence, not all heat is lost from the system, and a temperature above the adiabatic temperature corresponding to a given mixture composition can be reached in the combustion zone. Theoretically, mixtures of arbitrarily lean composition can be burned in this way. This can be achieved by lengthening the heat exchange segment between the countercurrent channels, as well as by increasing the thermal heat exchange through the separating wall. However, different additional side effects, such as heat loss to the external environment, for example, or inadequate heat exchange between channels, can reduce the burner efficiency.

A significant number of investigations on the subject of superadiabatic burners have been reported over the past two decades [31, 32, 33, 34, 35, 36, 37, 38, 39, 40, 41, 42]. Most of the studies were based on one-step Arrhenius-type kinetics, a model for which there is no flammability limit, as mentioned above. More complex kinetics were used in [35] for propane-air mixtures, or in [41] for the production of hydrogen-rich syngas from methanol, for example. Comprehensive reviews regarding these small-scale combustion devices can be found in [43, 44, 45, 46, 47, 48] and in a very recent survey [49].

Recently, a two-step chain-branching kinetics model has been used in numerical and analytical studies for heat recirculating countercurrent burners [50, 51]. In these studies, a narrow-channel one-dimensional approximation was introduced and used for channels thermally connected to each other through a conductive segment of the separating wall. Although this one-dimensional approximation describes the process satisfactorily for fairly narrow channels [42], a study of the impact of the channel width on the efficiency of the burner is required. The present work attempts to fill this gap.

The article is organized as follows: Section 2 presents the problem statement. Section 3 describes the asymptotic approximations used to obtain numerical solutions. Section 4 briefly describes the numerical methods used.

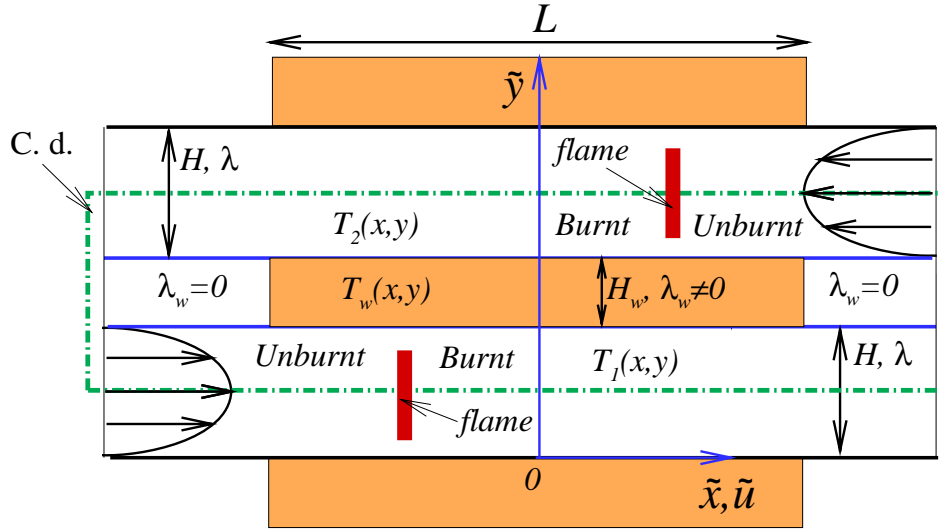


Figure 1: Sketch of the problem, coordinate system and opposite-velocity profiles in two channels; the computational domain is marked with a dash-dotted line rectangle.

Section 5 presents the results obtained, while the last section presents the conclusions drawn by the authors.

## 2. Formulation

The device under consideration consists of a periodic system of identical channels of width  $H$  separated by walls of width  $H_w$ . A mixture of fuel and oxidizer flows in adjacent channels in opposite directions. The analysis presented below is limited to cases where the flow rates are equal in all channels. A schematic representation is given in Fig. 1 where  $\tilde{x}$ ,  $\tilde{y}$  denote the longitudinal and wall-normal coordinates, respectively. We assume that the heat exchange between the channels occurs in a wall segment of length  $L$ . Assuming a periodic array of countercurrent channels, the domain under consideration is reduced to two adjacent channels. When necessary, the channels with the flow direction to the right and to the left will be designated as 1 and 2, respectively.

For simplicity, we assume also that the channel walls are adiabatic outside the heat exchange segment. When the length of the heat exchange zone is

sufficient, the thermal conditions on the walls outside this segment are of no importance. The initial (upstream in every channel) temperature is equal to  $T_0$  and the initial mass fraction of the combustible substance is  $F_0$ . The mixture is assumed to be deficient in fuel while the mass fraction of oxidizer, which is in excess, remains nearly constant.

According to the diffusive-thermal model applied in the present study, the density of the mixture  $\rho$ , the average heat capacity  $c_p$ , the thermal conductivities of the gas and the wall material,  $\lambda$  and  $\lambda_w$ , and the molecular diffusivities of the fuel and radical species in the mixture,  $\mathcal{D}_F$  and  $\mathcal{D}_Z$ , are all constant.  $\mathcal{D}_T = \lambda/\rho c_p$  stands for the thermal diffusivity, and is also constant within this model. Consequently, the flow field is not affected by combustion and the flow velocity is given by the parabolic Poiseuille flow in every channel.

In the present study we use the two-step chain-branching kinetic mechanism initially developed in [3, 4, 5, 6]. This chemistry includes the auto-catalytic reaction,  $F + Z \rightarrow 2Z$ , and the recombination reaction,  $Z + M \rightarrow P + M + Q$ , with reaction rates given by

$$\begin{aligned}\Omega_B &= A_B(\rho\tilde{F}/W_F) \cdot (\rho\tilde{Z}/W_Z) e^{-E/R_gT}, \\ \Omega_C &= A_C(\rho\tilde{Z}/W_Z) \cdot (\rho/W),\end{aligned}\tag{1}$$

where  $\Omega_B$  is the chain-branching reaction rate, assumed to be thermally sensitive with activation energy  $E$ , and  $\Omega_C$  is the completion or recombination reaction rate with zero activation energy. As usual, all the heat,  $Q$ , is released in the completion step. In Eq. (1)  $A_B$  and  $A_C$  represent the reaction rate constants,  $\rho$  is the density,  $T$  is the temperature,  $\tilde{F}$  and  $\tilde{Z}$  are the mass fractions of fuel and radicals,  $R_g$  is the universal gas constant, and  $W_F$ ,  $W_Z$  and  $W$  are the fuel, radical and mean molecular weights, respectively.

Within the framework of the above simplifications, the governing equations are represented by the conservation laws for the mass fractions of fuel and radicals, as well as for the energy. For brevity, the equations are written down for only one channel.

$$\frac{\partial\tilde{F}}{\partial\tilde{t}} + \tilde{v}\frac{\partial\tilde{F}}{\partial\tilde{x}} = \mathcal{D}_F\left(\frac{\partial^2\tilde{F}}{\partial\tilde{x}^2} + \frac{\partial^2\tilde{F}}{\partial\tilde{y}^2}\right) - W_F\frac{\Omega_B}{\rho},\tag{2}$$

$$\frac{\partial\tilde{Z}}{\partial\tilde{t}} + \tilde{v}\frac{\partial\tilde{Z}}{\partial\tilde{x}} = \mathcal{D}_Z\left(\frac{\partial^2\tilde{Z}}{\partial\tilde{x}^2} + \frac{\partial^2\tilde{Z}}{\partial\tilde{y}^2}\right) + W_Z\frac{\Omega_B}{\rho} - W_Z\frac{\Omega_C}{\rho},\tag{3}$$

$$\frac{\partial T}{\partial \tilde{t}} + \tilde{v} \frac{\partial T}{\partial \tilde{x}} = \lambda \left( \frac{\partial^2 T}{\partial \tilde{x}^2} + \frac{\partial^2 T}{\partial \tilde{y}^2} \right) + \frac{Q}{c_p} \cdot \frac{\Omega_C}{\rho}, \quad (4)$$

The characteristic time and length,  $t_c$  and  $L_c$ , used to define the dimensionless variables are chosen from the following relations

$$t_c \mathcal{D}_T / L_c^2 = 1, \quad t_c \rho A_C / W = 1. \quad (5)$$

The characteristic quantities  $t_c$  and  $L_c$  determine the scale of the characteristic velocity  $U_c = L_c / t_c = \sqrt{\rho A_C \mathcal{D}_T / W}$ . The parameters  $a = H / L_c$  and  $\ell = L / L_c$  stand for the dimensionless channel width and the dimensionless length of the heat exchange segments, respectively. The dimensionless wall thickness is defined as  $h_w = H_w / H$ .

Dimensionless temperatures in the gas phase and in the solid material are defined here as  $\theta = (T - T_0) / (T_c - T_0)$ ,  $\theta_w = (T_w - T_0) / (T_c - T_0)$ , both based on the branching temperature  $T_c$ . This temperature is usually known as an "inhomogeneous" crossover temperature and has been widely discussed in [3, 4, 5, 6]. The branching temperature  $T_c$  is determined by the relation  $\Omega_B = \beta^2 \Omega_C$  evaluated at the initial fuel mass fraction  $F_0$ , where  $\beta = E(T_c - T_0) / R_g T_c^2$  is the Zel'dovich number based on  $T_c$ . It is important to see that the radical mass fractions  $Z$  in  $\Omega_B$  and  $\Omega_C$  are canceled out and, finally,  $T_c$  is defined by the equation

$$\frac{A_B}{A_C} \frac{W}{W_F} F_0 = \left\{ \frac{E}{R_g} \cdot \frac{T_c - T_0}{T_c^2} \right\}^2 \exp \left\{ \frac{E}{R_g T_c} \right\}. \quad (6)$$

When studying combustion in narrow channels, it is convenient to use different scales for the longitudinal and transverse coordinates,  $x = \tilde{x} / L_c$ ,  $y = \tilde{y} / H$ . This allows to investigate the narrow channel limit,  $a \rightarrow 0$ , when the governing equations are reduced to the one-dimensional form. Using  $F_0$  and  $Z_0 = (W_Z / W_F) F_0$  to normalize the mass fractions of fuel and radicals, namely  $F = \tilde{F} / F_0$  and  $Z = \tilde{Z} / Z_0$ , the dimensionless gas phase equations, to be considered for  $0 < y < 1$  (the channel with rightward moving mixture) and  $1 + h_w < y < 2 + h_w$  (the channel with leftward moving mixture), take the form

$$\frac{\partial F}{\partial t} + mv(y) \frac{\partial F}{\partial x} = \frac{1}{Le_F} \left( \frac{\partial^2 F}{\partial x^2} + \frac{1}{a^2} \frac{\partial^2 F}{\partial y^2} \right) - \omega, \quad (7)$$

$$\frac{\partial Z}{\partial t} + mv(y) \frac{\partial Z}{\partial x} = \frac{1}{Le_Z} \left( \frac{\partial^2 Z}{\partial x^2} + \frac{1}{a^2} \frac{\partial^2 Z}{\partial y^2} \right) + \omega - Z, \quad (8)$$

$$\frac{\partial \theta}{\partial t} + mv(y) \frac{\partial \theta}{\partial x} = \left( \frac{\partial^2 \theta}{\partial x^2} + \frac{1}{a^2} \frac{\partial^2 \theta}{\partial y^2} \right) + qZ, \quad (9)$$

where

$$\omega = \beta^2 F Z \exp \left\{ \frac{\beta(\theta - 1)}{1 + \gamma(\theta - 1)} \right\}. \quad (10)$$

The dimensionless Poiseuille profiles in the two channels have opposite directions,

$$v(y) = \begin{cases} 6y[1 - y], & 0 < y < 1, \\ -6[y - (1 + h_w)][2 + h_w - y], & 1 + h_w < y < 2 + h_w. \end{cases} \quad (11)$$

Inside the heat exchange wall segment, the equation for temperature is

$$\frac{\partial \theta_w}{\partial t} = \alpha \left( \frac{\partial^2 \theta_w}{\partial x^2} + \frac{1}{a^2} \frac{\partial^2 \theta_w}{\partial y^2} \right), \quad (12)$$

to be solved for  $1 < y < 1 + h_w$ .

The dimensionless parameters appearing in the above equations are as follows:  $m = U/U_c$  is the dimensionless flow velocity,  $q = QF_0/c_p(T_c - T_0)W_F$  is the dimensionless heat of reaction,  $\gamma = (T_c - T_0)/T_c$  is the heat release parameter,  $Le_F = \mathcal{D}_T/\mathcal{D}_F$  and  $Le_Z = \mathcal{D}_T/\mathcal{D}_Z$  are the Lewis numbers of the fuel and radicals and  $\alpha = (\lambda_w/\lambda) \cdot [(\rho_0 c_p)/(\rho_w c_w)]$  represents the dimensionless thermal diffusivity of the wall inside the heat exchange segment, with  $\rho_w$  and  $c_w$  the density and the heat capacity of the wall material. Note for clarity that, within the framework of the kinetic model used, the dimensionless adiabatic temperature, the temperature of the mixture assuming the complete chemical consumption of fuel, is equal to  $q$ .

For simplicity, we will consider a periodic system of channels. It is well known that for sufficiently narrow channels the flame structure is always symmetrical with respect to the midplane of the channel, provided that the boundary conditions are the same on opposite walls [53, 54]. This makes it possible to establish symmetrical boundary conditions at the every midplane of the two adjacent channels to be considered. With this symmetry conditions, Eqs. (8)-(12) are to be solved subject to the following boundary conditions:

- along the solid walls, at  $y = 1$  and  $y = 1 + h_w$ ,

$$\frac{\partial F}{\partial y} = \frac{\partial Z}{\partial y} = 0, \quad \theta = \theta_w, \quad \frac{\partial \theta}{\partial y} = \begin{cases} \frac{1}{2} b a^2 h_w \frac{\partial \theta_w}{\partial y}, & 0 < x < \ell, \\ 0, & x < 0, x > \ell; \end{cases} \quad (13)$$

- along the midplane of the channels, at  $y = 1/2$  and  $y = 3/2 + h_w$ ,

$$\frac{\partial \theta}{\partial y} = \frac{\partial F}{\partial y} = \frac{\partial Z}{\partial y} = 0; \quad (14)$$

- along the lateral conducting wall segments, at  $1 < y < 1 + h_w$  and  $x = 0, \ell$ ,

$$\frac{\partial \theta_w}{\partial x} = 0; \quad (15)$$

- far upstream the channels,

$$\theta \rightarrow 0, \quad F \rightarrow 1, \quad Z \rightarrow 0; \quad (16)$$

- at the outlet of the channels,

$$\frac{\partial \theta}{\partial x} = \frac{\partial F}{\partial x} = \frac{\partial Z}{\partial x} = 0. \quad (17)$$

The heat exchange parameter appearing in Eq. (13) is defined as

$$b = \frac{2\lambda_w}{\lambda a^2 h_w} = 2 \frac{\lambda_w}{\lambda} \cdot \frac{L_c^2}{H H_w}. \quad (18)$$

The purpose of presenting the coefficient  $b$  in this form is to consider the various limiting cases described in next section.

In the following, the flame position  $x_f$  is defined as the point along the channel midplane at which the radical mass fraction  $Z$  reaches its maximum value. As follows from Eq. (9), this point corresponds to the point of maximum heat release. For most of the results presented below, the distributions of temperature and mass fractions in adjacent channels turn out to be symmetric with respect to the  $x = \ell/2$  plane. To identify the combustion mode in this case, the position of the flame will be indicated only in the channel where reactants flow to the right. In the adjacent channel, the position of the flame will be  $x'_f = \ell - x_f$ . The cases of non-symmetric solutions will be indicated separately.

All the calculations reported below were carried out for  $Le_F = 1$ , and  $Le_Z = 0.3$ . The values of the Zeldovich and heat release parameters were fixed at  $\beta = 10$  and  $\gamma = 0.7$  in most cases, unless otherwise specified. It should be noted that in the limit of  $\beta \rightarrow \infty$ , the calculation of the dimensionless heat of reaction corresponding to the flammability limit gives

$q = q_f = 1$ . As pointed out in [50], for finite values of the Zel'dovich number, this quantity is slightly less than unity and, in the general case, depends on  $\beta$ ,  $\gamma$  and  $Le_F$ . In particular, for  $\beta = 10$ ,  $\gamma = 0.7$  and  $Le_F = 1$ , the values used in this work, we have  $q_f \approx 0.8827$ , see Appendix.

### 3. Limiting cases $a \rightarrow 0$ and $h_w \rightarrow 0$ (with $a = O(1)$ )

The heat exchange coefficient  $b$  given by Eq. (18) and appearing in Eq. (13) is scaled with  $h_w$  and  $a^2$  in order to make it easier to consider the following limiting cases. The first limiting case is the narrow-channel approximation for which the governing equations are reduced to the spatially one-dimensional form. This limit is set by the condition  $a = H/L_c \rightarrow 0$ . It should be noted that due to  $h_w = O(1)$ , the width of the separating wall is considered to be of the same order as the width of the channel,  $H_w \sim H$ . The resulting equations are obtained as the first term in the  $a^2$  expansion. The applicability of this limit was investigated before in [42] by using an Arrhenius-type kinetics and it is not repeated here. In their final shape, the governing equations are reduced to their one-dimensional counterpart

$$\frac{\partial F_i}{\partial t} \pm m \frac{\partial F_i}{\partial x} = \frac{1}{Le_F} \frac{\partial^2 F_i}{\partial x^2} - \omega_i, \quad (19)$$

$$\frac{\partial Z_i}{\partial t} \pm m \frac{\partial Z_i}{\partial x} = \frac{1}{Le_Z} \frac{\partial^2 Z_i}{\partial x^2} + \omega_i - Z_i, \quad (20)$$

$$\frac{\partial \theta_i}{\partial t} \pm m \frac{\partial \theta_i}{\partial x} = \frac{\partial^2 \theta_i}{\partial x^2} + q Z_i \mp b(\theta_1 - \theta_2). \quad (21)$$

Here the indices  $i = 1$  and  $2$  denote channels with rightward and leftward mixture flow directions, together with the upper and lower signs in the equation, respectively. It is interesting to note that the same equations are obtained in the considered limit if the constant density assumption is not made. Indeed, in practice the procedure is reduced to averaging across the channel and the variables in Eqs. (19)-(21) are average variables when the total flow rate through each channel (equal to  $m$ ) is fixed.

Although this study considers a periodic system of channels, one can easily extend it to the case of only two counter flow channels, assuming adiabaticity for the walls in contact with the external environment. To do this, following the asymptotic consideration outlined in [42], the factor 2 must be excluded from Eq. (18), since the integration across the channel must be

carried out over its entire section, and not only over a half section, as in the case of a periodic system of channels.

The second limiting case considered here is the limit  $h_w \rightarrow 0$ , while the dimensionless width of the channels,  $a$ , remains formally of order unity. Using the scaled variable  $\hat{y} = (y - 1)/h_w$ , the temperature equation in the conducting segment becomes

$$\frac{\partial \theta_w}{\partial t} = \alpha \left( \frac{\partial^2 \theta_w}{\partial x^2} + \frac{1}{a^2 h_w^2} \frac{\partial^2 \theta_w}{\partial \hat{y}^2} \right). \quad (22)$$

Assuming (formally) that all parameters are of order unity and  $h_w \ll 1$ , the wall temperature is expanded in power series of  $h_w^2$ , i.e. in the form  $\theta_w = \theta_w^{(0)} + h_w^2 \theta_w^{(1)} + \dots$ . Finally, the leading order solution for the wall temperature reads

$$\theta_w^{(0)} = \theta_1 + (\theta_2 - \theta_1) \cdot \frac{y - 1}{h_w}, \quad (23)$$

where continuity of the temperature field on the solid surface was used. Substituting this solution into Eq. (13) gives the boundary condition in the form

$$\begin{aligned} 0 < x < \ell : \quad \left. \frac{\partial \theta_1}{\partial y} \right|_{y=1-} &= \frac{1}{2} b a^2 (\theta_2 - \theta_1), \quad \left. \frac{\partial \theta_2}{\partial y} \right|_{y=1+} = \frac{1}{2} b a^2 (\theta_2 - \theta_1), \\ x < 0, x > \ell : \quad \left. \frac{\partial \theta_1}{\partial y} \right|_{y=1-} &= \left. \frac{\partial \theta_2}{\partial y} \right|_{y=1+} = 0. \end{aligned} \quad (24)$$

Thus, it can be seen that the representation of the boundary conditions in the form given by Eq. (13) is convenient to compare the results obtained in these limiting cases with more general ones. We also note that if we take the limit  $a \rightarrow 0$  in the governing equations and boundary conditions (24), then the formulation takes the one-dimensional form given by Eqs. (19)-(21).

In the asymptotic expansions presented above, all parameters, with the exception of the parameter used for the asymptotic expansion ( $a$  for the first case and  $h_w$  for the second), should be considered (formally) as being of order of unity. It should be noted that the approximations considered above are not the only possible ones. In [52], the approximation of a highly conductive wall segment corresponding to the limit  $\lambda_w/\lambda \rightarrow \infty$  was considered. In this case, the high thermal conductivity of the wall leads to a uniform wall temperature whose value must be determined from the wall heat flux balance. However, that limiting case will not be considered in this paper.

## 4. Numerical treatment

All computations were carried out in a finite domain,  $x_{min} < x < x_{max}$ , with  $x_{min} < 0$  and  $x_{max} > \ell$ . Typical values were  $x_{min} = -10$  and  $x_{max} = \ell + 10$ . The spatial derivatives in all the governing equations were discretized on a uniform grid using second order, three-point central finite differences. The typical number of points in each direction was  $N_x = 2000$  and  $N_y = 100$  in each channel. These values were also doubled to provide resolution validation. The  $y$ -derivatives appearing in the wall boundary conditions were also discretized with second order accuracy.

The steady counterpart ( $\partial/\partial t = 0$ ) of the governing equations was solved using a Gauss-Seidel method with over-relaxation. Two iterating methods were used. In the first method, the values of all parameters were fixed. Only solutions belonging to the stable branches could be calculated using this method. In the second method, the temperature was fixed at a point  $x = x_*$  (and  $y = y_*$  for two-dimensional calculations) in the rightward flow channel imposing  $\theta_1 = \theta_*$  while the value of the flow rate  $m$ , for example, was calculated iteratively (also with a Gauss-Seidel procedure). The numerical values of  $\theta_*$  used were between 0.7 and 1. Most of the calculations were carried out with  $y_* = 0.5$  (middle of the first channel), although it is obvious that the results should not depend on  $(x_*, y_*)$ , which was confirmed. Namely, for each selected set  $(x_*, y_*)$ , the value of  $m$  and the position of the flame were calculated, and the dependencies of  $x_f$  on  $m$  coincided for different  $y_*$ , as it should be. The second numerical method allows to find unstable solutions, which is important for the exact determination of the regions of existence of steady-state regimes.

Although time-dependent dynamics was not the subject of study, some unsteady calculations were also carried out mainly to study the stability of steady-state solutions. These calculations were carried out using an explicit scheme of the first order of accuracy. The time step varied from  $10^{-4}$  to  $10^{-6}$ . The presence of a sharp dependence of the reaction rate on temperature required the use of a sufficiently small time step, which allowed the use of the explicit time method.

## 5. Results

Before proceeding to the description of steady-state solutions, it should be noted that two solutions were obtained for each value of the flow rate,

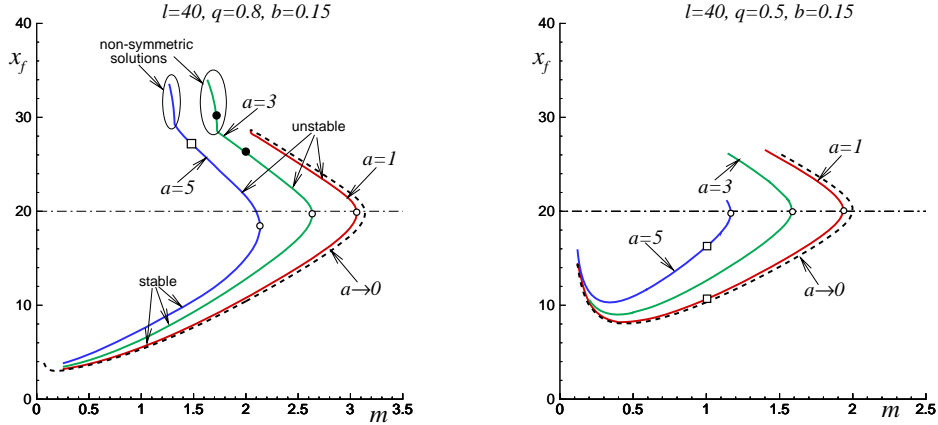


Figure 2: The flame position  $x_f$  in the rightward flowing channel versus the flow rate  $m$  plotted for  $q = 0.8$  (left plot),  $q = 0.5$  (right plot) and various  $a$ ; all curves calculated for  $\ell = 40$  and  $b = 0.15$ . Dashed lines show the asymptotic case  $h_w \rightarrow 0$ ; open circles mark the maximum values of the flow rate; filled circles (left plot) correspond to initial conditions for the simulations presented in Fig. 3. The marked segments correspond to non-symmetric solutions, of which an example is shown in Fig. 8.

with other parameters fixed. The typical dependence of the steady-state flame position on the flow rate showed the presence of turning points located near the middle of the heat exchange segment, as can be seen in Fig. 2, for example, where the turning points are marked with open circles on the presented curves. It should be noted that the results presented in [50, 51] were obtained on the basis of an analytical method, in which finding the flame position was reduced to finding the roots of an algebraic equation. This made it possible to obtain, for example, closed curves for the position of the flame versus the flow rate. In the case of the numerical solution of the equations, the approach taken in the present study, the calculation of some parts of closed curves presents significant numerical difficulties due to the rigidity of the corresponding calculations. However, it should be noted that these difficulties are associated only with the parts of the curves corresponding to unstable solutions (see below). For stable solutions, no difficulties were observed.

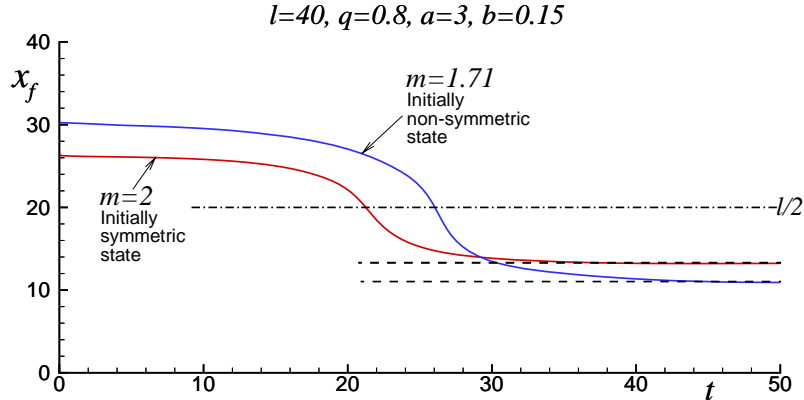


Figure 3: Examples illustrating evolutions of the flame position,  $x_f$ , for  $\ell = 40$ ,  $q = 0.8$ ,  $b = 0.15$ ,  $a = 3$  in the rightward flow direction channel; the initial conditions correspond to the states lying above the turning point in Fig. 2 (marked with filled circles) for  $m = 2$  (initially symmetric state) and  $m = 1.71$  (initially non-symmetric state). Horizontal dashed lines mark the corresponding stable states.

### 5.1. The limiting case $h_w \rightarrow 0$

Let us consider the case of the thin channel wall approximation by setting  $h_w \rightarrow 0$  when the temperature boundary conditions on the wall are reduced to Eq. (24). The steady-state flame position  $x_f$  (in the rightward flowing mixture channel) versus the flow rate  $m$  is shown in Fig. 2 for  $q = 0.8$  (left plot),  $q = 0.5$  (right plot) and various values of the dimensionless width  $a$ . These two values of  $q$  correspond to a mixture with a fuel content below the flammability limit. The remaining parameters are fixed at  $\ell = 40$ ,  $b = 0.15$ ,  $Le_F = 1$  and  $Le_Z = 0.3$ . The curves drawn with dotted lines show limiting cases corresponding to  $a \rightarrow 0$  and based on Eqs. (19)-(21). These results show that as the channel width decreases, the results tend to the limiting case  $a \rightarrow 0$ .

It can be seen in Fig. 2 that as the flow rate increases, the flame approaches the middle of the heat exchange segment  $\ell/2$ , near which there are turning points marked with open circles. If we follow further, then the flame continues to move along the channel downstream, but the corresponding flow rate decreases, that is, for each  $m$  there are two solutions. The turning point determines the maximum flow rate value above which the combustion process is impossible (for these fixed values of the parameters). It is interesting

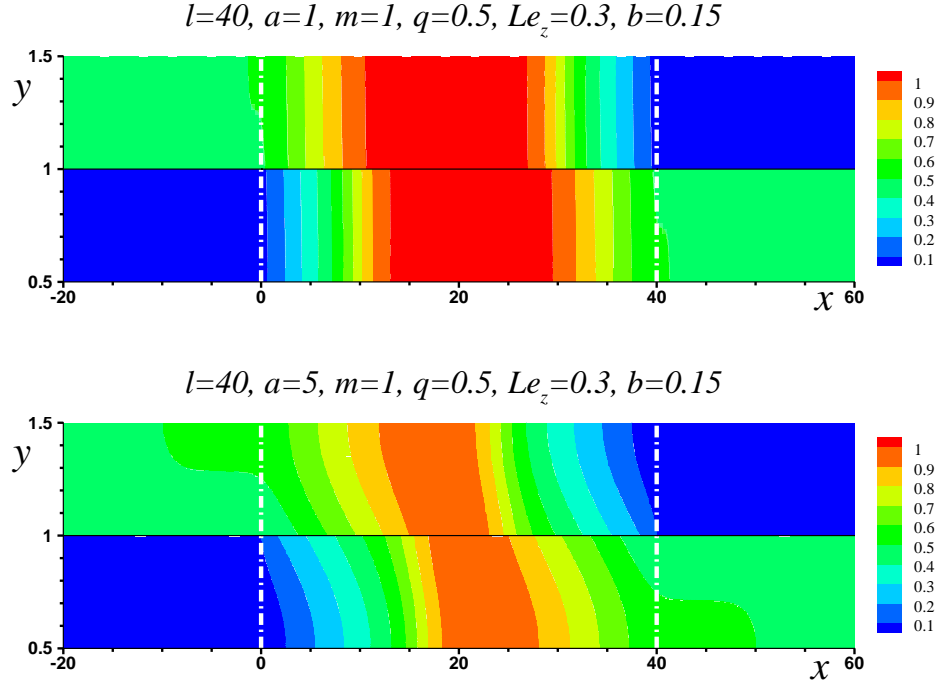


Figure 4: Temperature contour plots illustrating the states corresponding to the points indicated with open squares in Fig. 2 (right) for  $q = 0.5$ .

to note that for small  $a$ , the turning point is close to the middle of the heat exchange segment,  $x \approx \ell/2$ , while for larger  $a$ , the critical value is reached before the point  $x = \ell/2$ . In all likelihood, this is due to the increase in the flame curvature in wider channels. Indeed, the position of the flame,  $x_f$ , is determined, for convenience, along the middle of the channel. For this reason, this value may not fully reflect the flame structure in wider channels.

Global stability analysis of the obtained steady-state solutions is not the subject of the present study. However, we can signal, parenthetically, that all the (considered) states corresponding to flame positions lying above the turning point (in the first channel) are unstable. Time-dependent calculations revealed that in all cases where steady solutions corresponding to the upper branch (above the turning point in Fig. 2) were chosen as the initial condition, then the typical time evolution illustrated in Fig. 3 took place, that is, at a fixed flow rate, the solution lying on the lower branch was ap-

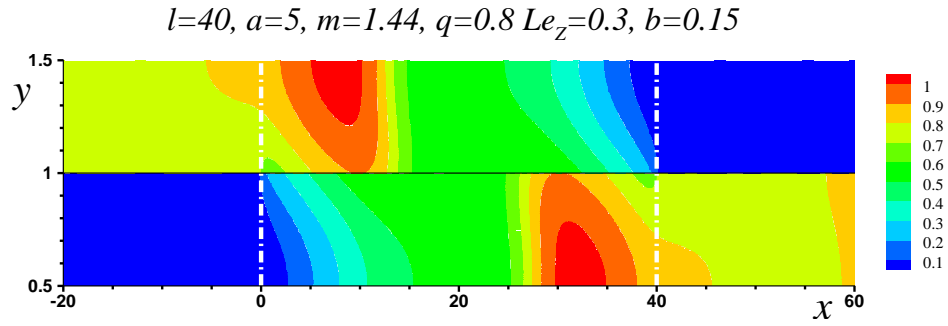


Figure 5: Temperature contour plots illustrating the unstable state corresponding to the point indicated with open square in Fig. 2 (left)

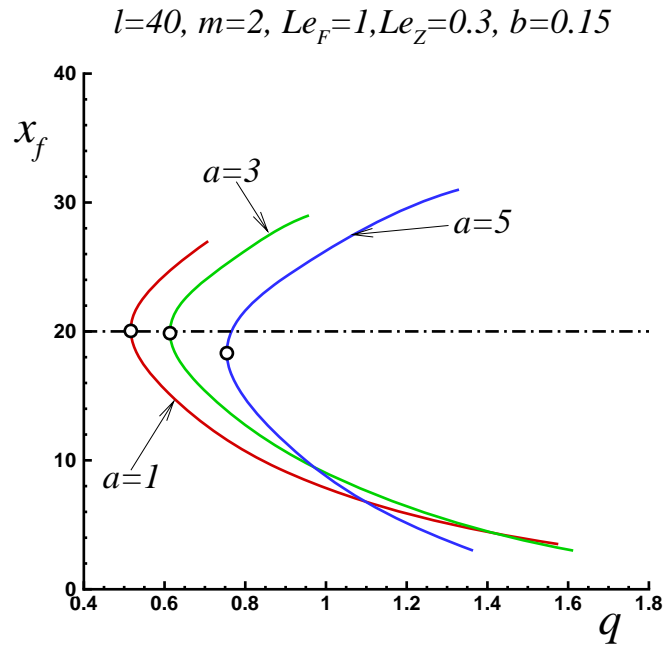


Figure 6: The dependence of  $x_f$  on  $q$  calculated for  $m = 2$  and different values of the channel width  $a$ . Open circles mark the critical values of  $q$  below which combustion is impossible (for a given value of  $m$ ).

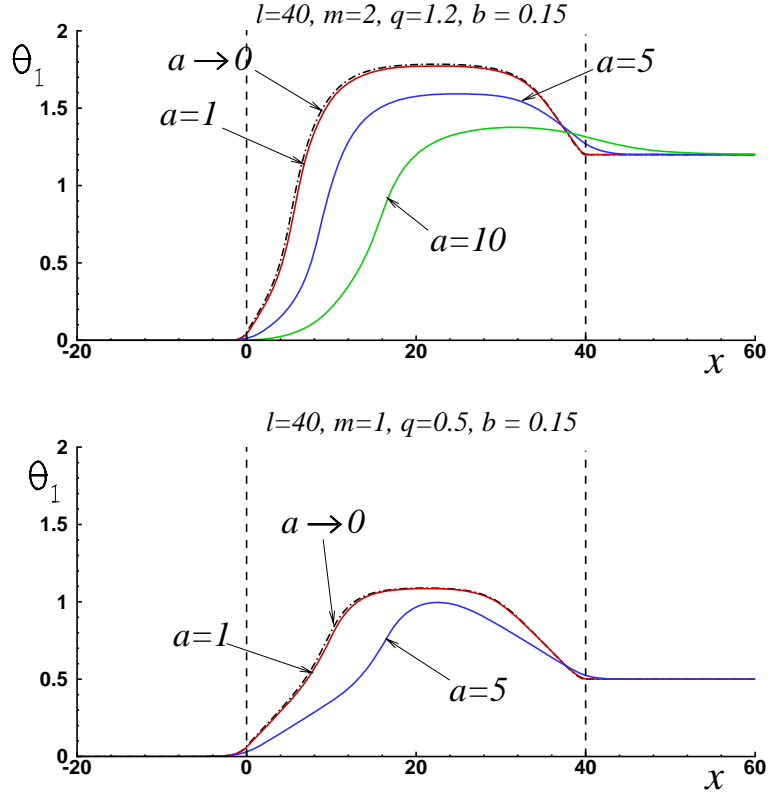


Figure 7: Temperature distributions along the channel axis, for different values of  $a$  calculated for  $m = 2$ ,  $q = 1.2$  (upper plot) and  $q = 0.5$  (right plot); the dimensionless heat of reaction corresponding to the flammability limit is  $q_f = 0.8827$  for  $\beta = 10$ ,  $\gamma = 0.7$  and  $Le_F = 1$ .

proached. The initial conditions for the time evolution curves shown in Fig. 3 correspond to the filled circles in Fig. 2 (left), for  $\ell = 40$ ,  $q = 0.8$ ,  $b = 0.15$ ,  $a = 3$ . The case with  $m = 2$  corresponds to a symmetric initial condition, while for the case with  $m \approx 1.71$  the initial conditions are not symmetric. It can be seen that after the flame transition period, the position of the flame in the first channel approaches the steady state with  $x_f < \ell/2$ .

Note that, at least for the considered range of parameters, the instability has a monotonic character, i.e. no oscillatory dynamics was observed. This result agrees with the stability analysis reported in [50] carried out analytically within the one-dimensional approximation. Of course, selected

time-dependent calculations cannot replace a rigorous linear stability analysis, which will be reported somewhere else.

Fig. 4 compares the temperature distributions in the channels calculated for two channel widths with  $a = 1$  and  $a = 5$ , both for  $q = 0.5$ . The heat exchange segment is marked in the figure with white vertical dash-dotted lines. The distributions correspond to the values marked with open squares in Fig. 2 (right plot), that is, to flow rates  $m = 1$ . It can be seen that for the case of the narrower channel,  $a = 1$ , the temperature distribution depends only weakly on the transverse coordinate, while for the wider channel,  $a = 5$ , the temperature varies in the transverse direction. The temperature distribution for the unstable solution belonging to the upper solution branch is illustrated in Fig. 5. This state corresponds to the point indicated by an open square for  $m \approx 1.44$  in Fig. 2 (left).

Shown in Fig. 6 are the dependencies of the position of the flame on the dimensionless heat of reaction  $q$  calculated for various values of  $a$ , all curves obtained for  $\ell = 40$ ,  $m = 2$  and  $b = 0.1$ . Open circles indicate critical values of  $q$  below which combustion in the device is impossible. It can be seen that as the channel width increases, the critical value also increases, that is, the efficiency of the heat exchanger decreases and a higher energy content of the fresh mixture is required to guarantee sustained combustion. Obviously, these critical values depend on the flow rate. The plotted curves correspond to  $m=2$  and for different values of the flow rate a different set of curves will be obtained. The behavior at different flow rates will depend on the combination of two effects. On one side, a higher flow rate will increase the flame burning speed, but on the other side it will also change the flame position, bringing it farther away in the channel and this will decrease the heat exchange between channels and therefore the efficiency of recirculation. In this sense, it can be seen again that for small  $a$ , the turning point, and therefore the point of minimum heat recirculation efficiency determining the critical  $q$  value, practically coincides with the middle of the heat exchange segment, while it occurs earlier for large values of  $a$ .

Temperature distributions along the channel axis are shown in Fig. 6 for cases with  $q = 1.2$  and  $q = 0.5$ . In the first case, the mixture composition remains above the flammability limit, while for the second it is below this limit, i.e. the adiabatic temperature is lower than the corresponding cross-over temperature. Nevertheless, the figure demonstrates that in both cases the temperature inside the heat-exchange segment reaches values exceeding the cross-over temperature and therefore a self-sustained flame exists, even

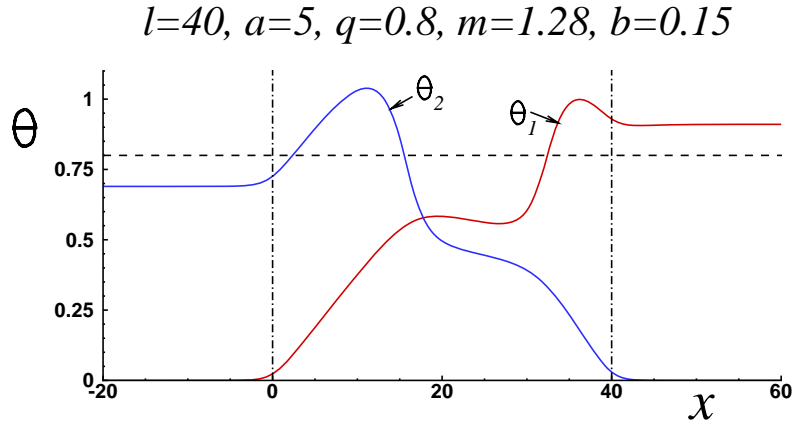


Figure 8: An example of the temperature distribution along the channel axis for a non-symmetric (unstable) solution, calculated for  $\ell = 40$ ,  $a = 5$ ,  $q = 0.8$  and  $m \approx 1.28$ .

far below the flammability limit. We also note that in the absence of heat loss, the temperature at the outlet of the burner is equal to the adiabatic temperature of the mixture,  $q$ , as it should follow from the energy conservation law.

One can see also, that the solutions on the upper (unstable) branch become non-symmetric with respect to the channel mid-axis. This area is marked in Fig. 2 (left). The temperature distributions along the channel axis corresponding to these non-symmetric solutions are illustrated in Fig. 8. It is interesting to note that the temperature of the mixture in channel 1 (rightward flowing channel) at the outlet of the heat exchange segment is higher than that in the adjacent channel. However, it can be seen that the average value over the two channels is still equal, as it should be, to the adiabatic temperature,  $\theta = 0.8$ . This value is marked with an horizontal dashed line in the figure. In all likelihood, the emergence of solutions that are not symmetric with respect to  $\ell/2$  is not related to the chain-branching kinetic model, since similar non-symmetric solutions were also observed for one-step Arrhenius kinetics [42]. We emphasize once again that these solutions are unstable.

The parametric interval in which the superadiabatic device can operate depends significantly on the properties of the separating wall. Within the model used, this is expressed by the value of the coefficient  $b$ . For  $b = 0.15$ ,  $a = 1$  and  $q = 0.5$  the flow rate should not exceed  $m \approx 1.95$  (see Fig. 2

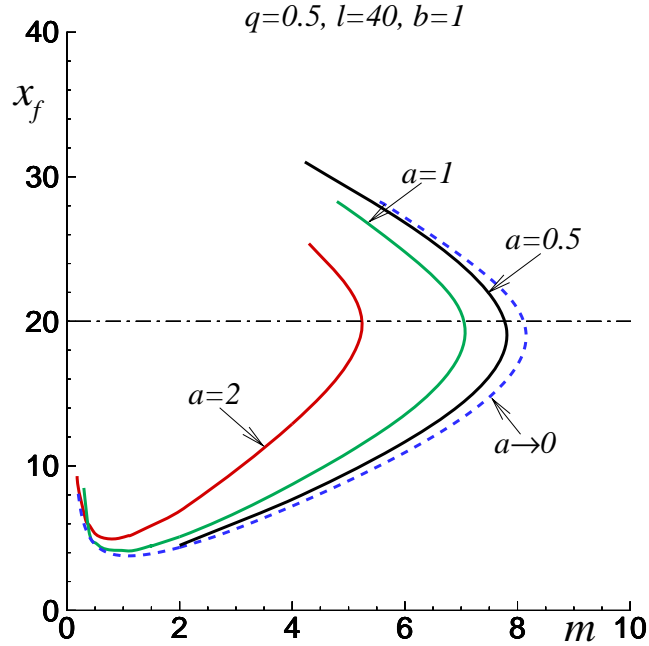


Figure 9: The dependence of the position of the flame in the channel on the flow rate for various  $a$ , for  $b = 1$ ,  $\ell = 40$  and  $q = 5$ . The limiting  $a \rightarrow 0$  solutions are shown by a dashed line.

(right)). Figure 9 shows the dependence of the flame position on the flow rate for cases calculated with a channel wall with  $b = 1$ . It can be seen that the maximum value for the flow rate is approaching  $m \approx 7$  for  $a = 1$ . Thus, a change in the wall parameter from  $b = 0.15$  to  $b = 1$  results in a large variation in the parametric range where self-sustained combustion can occur.

One of the main goals of the present study is to demonstrate that, with an adequate choice of dimensionless parameters, the limiting case of the narrow channel approximation,  $a \rightarrow 0$ , satisfactorily describes the behavior of the considered device. This was demonstrated for flammable mixtures, using one-step Arrhenius kinetics in [42]. Here, since we are using the chain-branching chemical model, we can extend this demonstration to ultra-lean mixtures, below the flammability limit. Figure 10 shows the position of the flame as

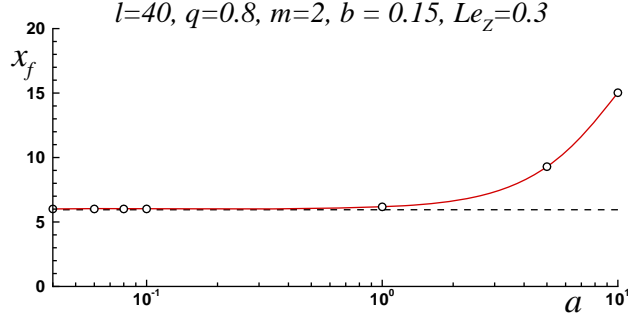


Figure 10: Flame position value obtained at different values of  $a$ , for  $\ell = 40$ ,  $q = 0.8$ ,  $m = 2$  and  $b = 0.15$ .

a function of the channel width, for  $\ell = 40$ ,  $q = 0.8$  and  $b = 0.15$  with a flow rate of  $m = 2$  for decreasing values of the channel width  $a$ , compared to the position predicted using the narrow channel limit equations ( $a \rightarrow 0$ ). It can be seen that the position of the flame in the channel approaches the asymptotic value obtained from the narrow channel approximation and that for values of the channel width as large as  $a = 1$  this approximation remains sufficiently accurate.

### 5.2. Influence of $h_w = O(1)$

All the results presented above were calculated within the limiting case  $h_w \rightarrow 0$ . For a finite wall thickness, it is necessary to solve, in addition to the gas equations, Eq. (12) for the temperature inside the wall. Figure 11 illustrates the temperature distribution for a device with a wall thickness equal to half the width of the channel,  $h_w = 0.5$ ,  $a = 3$ ,  $\ell = 20$ ,  $m = 3$ ,  $b = 2$  and  $q = 0.8$ . The top and bottom plots in Fig. 12 show the distributions of temperatures and mass fractions along the middle of the channels of the device for for  $q = 0.8$  with  $m = 3$  and  $q = 0.5$  with  $m = 0.8$ .

Fig. 13 compares the flame positions in the rightward channel plotted versus the flow rate for  $h_w = 0.5$  (solid line) and in the limiting case  $h_w \rightarrow 0$  (dotted line). It was important to verify that finite values of  $h_w$  affect only slightly the flame position and even for  $h_w = 0.5$  the coincidence of the curves is good. Of course such a good match is possible because of the definition of the heat transfer coefficient proposed in Eq. (13).

Fig. 14 shows the changes in flame position as a function of  $h_w$  calculated

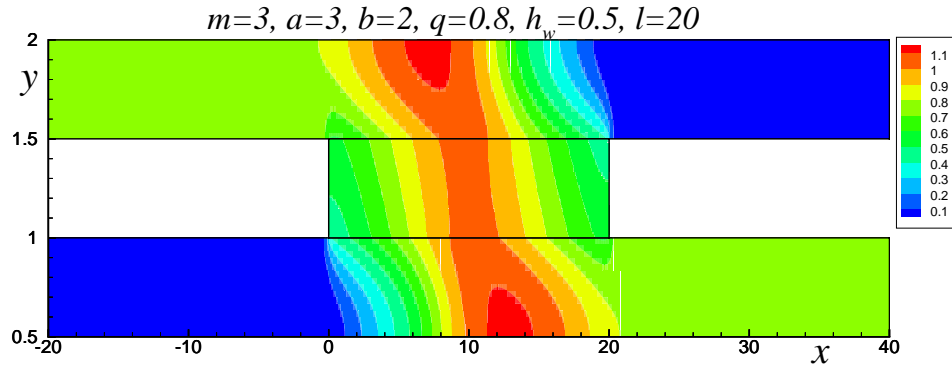


Figure 11: An example of temperature distribution in a device with a finite wall thickness,  $h_w = 0.5$ , plotted for  $m = 3$ ,  $\ell = 20$ ,  $a = 3$ ,  $b = 2$  and  $q = 0.8$ .

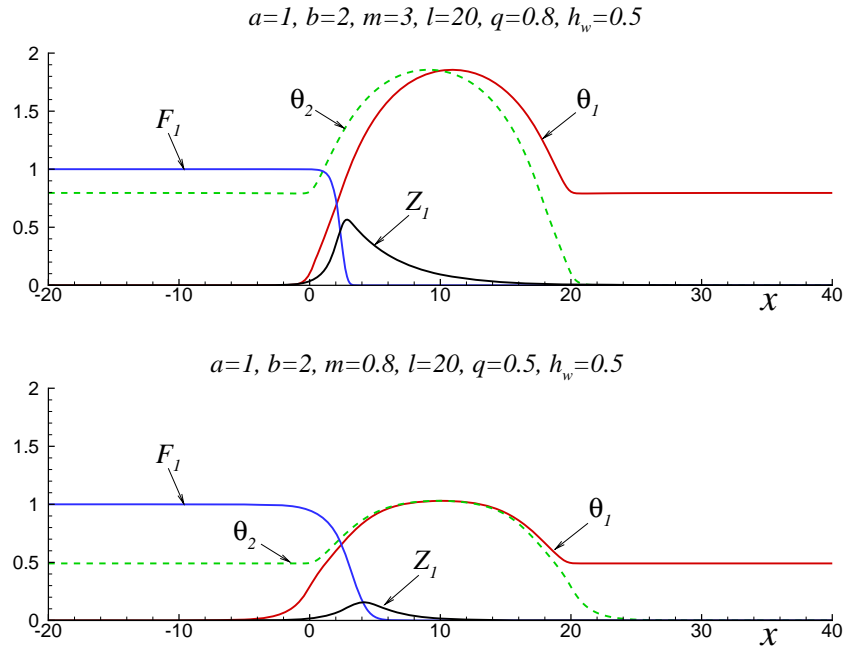


Figure 12: Examples of variable distributions along the channel axis calculated for  $h_w = 0.5$ , upper plot for  $q = 0.8$  and  $m = 3$ , lower plot for  $q = 0.5$  and  $m = 0.8$ .

for  $m = 3$ ,  $\ell = 20$ ,  $b = 2$  and various values of  $a$ . The curve calculated for  $a = 1$  demonstrates that even for  $h_w = O(1)$ , the deviations of the

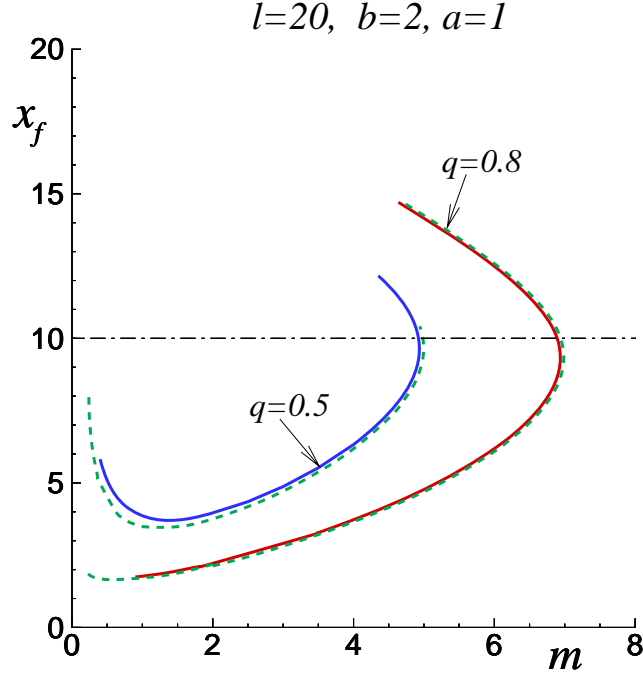


Figure 13: Dependence of the flame position in the channel on the flow rate  $m$  calculated for  $q = 0.8$  and  $0.5$ , all curves calculated with  $\ell = 20$ ,  $a = 1$ ,  $b = 2$ ; solid line -  $h_w = 0.5$ , dotted line -  $h_w \rightarrow 0$ .

flame position  $x_f$  from the asymptotic  $h_w \rightarrow 0$  value (dashed line) are small. However one can see that with increasing values of  $a$ , the upper values of  $h_w$  below which this difference remains small decrease. This can be explained by the fact that the dimensionless channel width is based on  $L_c$  determined by Eq. (5), namely  $a = H/L_c$ , while the dimensionless wall thickness is defined as  $h_w = H_w/H$ . If we re-scale the wall thickness using the length  $L_c$ , namely  $h'_w = H_w/L_c$ , then we have  $h'_w = a \times h_w$ . This means that, in fact,  $h'_w = h_w \times a$  plays the role of small parameter in the corresponding expansion.

## 6. Discussion and conclusions

The main characteristic of superadiabatic combustion burners is their property of reaching temperatures in the combustion zone significantly ex-

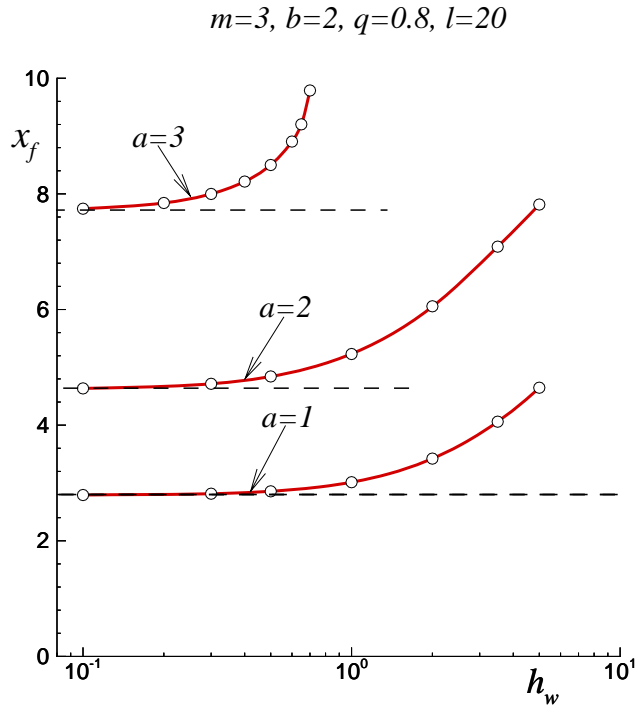


Figure 14: Dependence of the flame position on the value of the wall thickness, calculated for  $m = 3$ ,  $b = 2$ ,  $q = 0.8$  and  $\ell = 20$ . Dashed lines indicate the limiting values calculated in the limit  $h_w \rightarrow 0$ .

ceeding the temperature obtained after complete fuel burning, that is, the adiabatic temperature. This effect is achieved through heat recirculation in the device, when part of the heat from combustion remains inside the device and is not lost as hot combustion products are carried away from it. This valuable property allows the burning of extremely lean mixtures without external preheating. However, the performance of heat recirculation is highly dependent on the design of the device. The stability of combustion in these devices and the adequate values for their operation must be assessed in advance, at the design stage.

One of the difficulties in designing combustion devices is the large number of involved parameters, which makes difficult to find their adequate values for optimal burner operation. A possible approach to overcoming this obstacle is

the construction of simplified models, in which, with the help of asymptotic simplifications, the problem becomes more accessible for analysis. Possible asymptotic simplifications often arise from the fact that, with an adequate choice of scales for dimensional variables, the corresponding dimensionless formulation of the problem contains small/large dimensionless parameters that can be used to construct the asymptotic model. On the other hand, a situation often arises when the asymptotic model, obtained as a result of expansion using a small/large parameter, becomes applicable in a much wider range than is dictated by the requirement that the parameter be small/large. However, it should be noted that the applicability of the resulting model cannot be derived from the asymptotic procedure itself. This can only be done by comparing the results obtained from the full and the simplified models. An attempt to analyze this problem was made in the present work by applying asymptotic analysis to superadiabatic devices. The study focused on the consideration of two asymptotic cases, the case of a narrow channel and the case of a narrow wall, to simplify the problem statement by introducing effective parameters characterizing the heat recirculation in the device.

The heat recirculated through the separating walls and therefore the actual realization of high temperatures in the combustion zones is influenced by geometric parameters such as the length of the heat-exchange segment, the width of the channels, or the thickness of the walls; by physical parameters such as the thermal conductivity of the solid wall material; and by operating conditions such as the flow rate. All of these parameters and conditions define the existence of stable (or unstable) positions of the flame in the counter-flow channels within which the degree of heat recirculated varies. The asymptotic approximations attempt to reduce the number of these effective parameters, observing, for instance, an increase of the heat recirculation with the decrease of the ratio  $a = H/L_c$  or with the decrease of the ratio  $h_w = H_w/H$ .

This study was carried out on the basis of a chain-branching two-step kinetic mechanism in which the flammability limit is clearly included. This made it possible to demonstrate distinctly that the combustion of ultra-lean mixtures, that is, those for which the adiabatic temperature is below the cross-over temperature for a given mixture composition, is indeed possible in such devices. Theoretically, if the degree of heat recirculation is sufficiently high, then combustible mixtures with an arbitrarily small energy content can be burned under ideal conditions of no heat loss.

Besides, as another important result of this study, it can be emphasized that the application of the narrow-channel approximation and the narrow-

separating-wall approximation can be used, not only in the cases where the corresponding parameters are very small, but also for cases where they are of order unity. This opens up wider possibilities for using asymptotic 1D models to design and evaluate the performance of superadiabatic burners.

### Declaration of Competing Interest

The authors declare that they have no known competing financial interests or personal relationships that could have appeared to influence the work reported in this paper.

### Acknowledgment

This study was supported by MCIN with funding from European Union NextGenerationEU (PRTR-C17.I1) as well by grants #PID2019-108592RBC42AEI/10.13039/501100011033/ and #TED2021-129446-C42/AEI/10.13039/501100011033/NextGenerationEU/PRTR.

### Appendix. Flammability limit for finite $\beta$

The flammability limit for final  $\beta$  values was calculated in [12]. In that, a planar combustion wave was considered and the critical value of  $q = q_f$  corresponds to a zero value of the flame propagation velocity. The solution was obtained by the method of matched asymptotic expansions and will not be repeated here. As a result of this procedure, an algebraic equation to obtain the critical combustion wave temperature takes the form

$$\frac{\beta\theta_f}{(1 + \gamma(\theta_f - 1))^2} - Le_F[k(\theta_f) - 1] = 0, \quad (25)$$

where

$$k(\theta_f) = \beta^2 \exp \left[ \frac{\beta(\theta_f - 1)}{(1 + \gamma(\theta_f - 1))} \right].$$

Calculating  $\theta_f$  from Eq. (25), the critical heat of reaction corresponding to the flammability limit is given by

$$q_f = \frac{\theta_f \cdot k(\theta_f)}{k(\theta_f) - 1}. \quad (26)$$

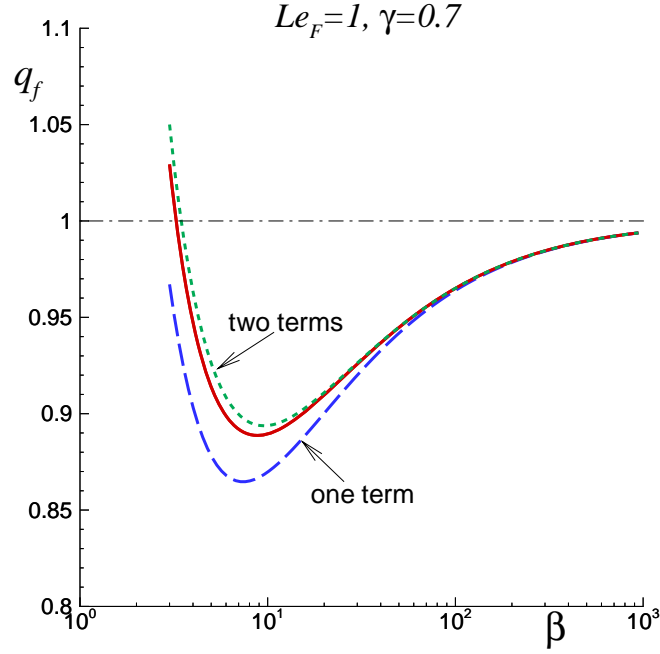


Figure 15: Dependence of the flammability limit critical value for the dimensionless heat of reaction on the Zel'dovich number, for  $\gamma = 0.7$  and  $Le_F = 1$ ; the solid line represents the solution of Eqs. (25) and (26), the lines with long and short dashes show one and two terms in the asymptotic expansion (27), respectively.

Eq. (25) does not have an explicit solution for  $\theta_f$ . However, one can obtain an asymptotic expression in the form

$$\begin{aligned}
 \beta \rightarrow \infty : \\
 \theta_f &= 1 - \frac{\ln(Le_F \cdot \beta)}{\beta} + \frac{a_2 \ln^2 \beta + a_1 \ln \beta + a_0}{\beta^2} + O(\beta^{-3} \ln^3 \beta), \\
 q_f &= 1 + \frac{Le_F - \ln(Le_F \cdot \beta)}{\beta} + \frac{b_2 \ln^2 \beta + b_1 \ln \beta + b_0}{\beta^2} + O(\beta^{-3} \ln^3 \beta),
 \end{aligned}
 \tag{27}$$

where

$$\begin{aligned}
 a_0 &= \gamma \ln^2 Le_F + (2\gamma - 1) \ln Le_F + Le_F, \\
 b_0 &= \gamma \ln^2 Le_F + (2\gamma(1 - Le_F) - 1) \ln Le_F + Le_F, \\
 a_1 &= 2\gamma(1 + \ln Le_F) - 1, \\
 b_1 &= 2\gamma(1 + \ln Le_F) - 1 - 2Le_F\gamma, \\
 a_2 &= b_2 = \gamma.
 \end{aligned}$$

Fig. 15 compares the values for the dimensionless critical heat of reaction corresponding to the flammability limit,  $q_f$ , obtained from the numerical solution of Eqs. (25)-(26) (solid line), with those obtained using one-term (long-dashed line) and two-terms (short-dashed line) expansions given by Eq. (27).

## References

- [1] F.A. Williams, *Combustion Theory*, 2nd ed., The Benjamin/Cummings Publishing Company, 1985, Chapter 8, p. 266.
- [2] V.N. Kurdyumov, M. Matalon, Effects of gas compressibility on the dynamics of premixed flames in long narrow adiabatic channels, *Combust. Theor. Model.* 20 (2016) 1046-1067.
- [3] J.W. Dold, R.W. Thatcher, A. Omon-Arancibia, J. Redman, From one-step to chain-branching premixed flame asymptotics, *Proc. Combust. Inst.* 29 (2002) 1519-1526.
- [4] J.W. Dold, R.O. Weber, R.W. Thatcher, A.A. Shah, Flame balls with thermally sensitive intermediate kinetics, *Combust. Theor. Model.* 7 (2003) 175-203.
- [5] J.W. Dold, J. Daou, R.O. Weber, Reactive-diffusive stability of planar flames with modified Zeldovich-Liñán kinetics, in "Simplicity, Rigor and Relevance in Fluid Mechanics. A volume in honor of Amable Liñán", Edited by F.J. Higuera, J. Jiménez, and J.M. Vega, eds., CIMNE, Barcelona, 2004.
- [6] J.W. Dold, Premixed flames modelled with thermally sensitive intermediate branching kinetics, *Combust. Theor. Model.* 11 (2007) 909-948.
- [7] Ya.B. Zeldovich, K teorii rasprostraneniya plameni, *Zh. Fiz. Khim.* 22 (1948) 27-49; Theory of flame propagation, English translation: *Nat. Advis. Comm. Aeronaut.* Technical Memorandum No. 1282, 1951.

- [8] Ya.B. Zeldovich, Chain reactions in hot flames - an approximate theory for flame velocity, *Kinetika i kataliz* 2 (1961) 305-318; English translation: *Int. Chem. Eng.* 2 (1962) 227-235.
- [9] Ya.B. Zeldovich, G.I. Barenblatt, V.B. Librovich, G.M. Mahviladze, *The Mathematical Theory of Combustion and Explosions*, Consultants Bureau, New York, 1985.
- [10] A. Liñán, A theoretical analysis of premixed flame propagation with an isothermal chain-branching reaction, Instituto Nacional de Técnica Aeroespacial Esteban Terradas (Madrid), USAFORS Contract No. E00AR68-0031, Technical Report No. 1, 1971.
- [11] G. Joulin, A. Liñán, G.S.S. Ludford, N. Peters, C. Schmidt-Laine, Flames with chain-branching/chain-breaking kinetics, *SIAM J. Appl. Math.* 45 (1985) 420-434.
- [12] V.N. Kurdyumov, D. Fenández-Galisteo, Asymptotic structure of premixed flames for a simple chain-branching chemistry model with finite activation energy near the flammability limit, *Combust. Flame* 159 (2012) 3110-3118.
- [13] V.V. Gubernov, H.S. Sidhu, G.N. Mercer, Combustion waves in a model with chain branching reaction and their stability, *Combust. Theor. Model.* 12 (2008) 407-431.
- [14] V.V. Gubernov, H.S. Sidhu, G.N. Mercer, A.V. Kolobov, A.A. Polezhaev, The effect of Lewis number variation on combustion waves in a model with chain-branching reaction, *J. Math. Chem.* 44 (2008) 816-830.
- [15] G.J. Sharpe, Effect of thermal expansion on the linear stability of planar premixed flames for a simple chain-branching model: The high activation energy asymptotic limit, *Combust. Theor Model.* 12 (2008) 717-738.
- [16] V.V. Gubernov, A.V. Kolobov, A.A. Polezhaev, H.S. Sidhu, G.N. Mercer, Pulsation instabilities of combustion waves in a chain-branching reaction model, *Int. J. Bifurcat. Chaos* 19 (2009) 873-887.

- [17] G.J. Sharpe, Thermal-diffusive instability of premixed flames for a simple chain-branching chemistry model with finite activation energy, *SIAM J. Appl. Math.* 70 (2009) 866-884.
- [18] V.V. Gubernov, A.V. Kolobov, A.A. Polezhaev, H.S. Sidhu, Stability of combustion waves in the Zeldovich-Liñán model, *Combust. Flame* 159 (2012) 1185-1196.
- [19] H. Zhang, Z. Chen, Bifurcation and extinction limit of stretched premixed flames with chain-branching intermediate kinetics and radiative loss, *Combust. Theor. Model.* 22 (2018) 531-553.
- [20] V.V. Gubernov, V.I. Babushok, S.S. Minaev, Phenomenological model of chain-branching premixed flames, *Combust. Theor. Model.* 23 (2019) 261-278.
- [21] D. Fernández-Galisteo, A.L. Sánchez, A. Liñán, F.A. Williams, The hydrogen-air burning rate near the lean flammability limit, *Combust. Theor. Model.* 13 (2009) 741-761.
- [22] D. Fernández-Galisteo, A.L. Sánchez, A. Liñán, F.A. Williams, One-step reduced kinetics for lean hydrogen-air deflagration, *Combust. Flame* 156 (2009) 985-996.
- [23] D. Fernández-Galisteo, A. Weiss, A.L. Sánchez, F.A. Williams, A one-step reduced mechanism for near-limit hydrogen combustion with general stoichiometry, *Combust. Flame* 208 (2019) 1-4.
- [24] "Chemical-Kinetic Mechanisms for Combustion Applications", San Diego Mechanism web page, Mechanical and Aerospace Engineering (Combustion Research), University of California at San Diego, Version 16-12-14. <http://web.eng.ucsd.edu/mae/groups/combustion/mechanism.htm>
- [25] D. Fernández-Galisteo, Numerical and asymptotic analysis of lean hydrogen-air deflagration, Universidad Carlos III de Madrid, 2009 Doctoral thesis (supervisor A.L. Sánchez Pérez).
- [26] J. Carpio, B. Li, D. Fernández-Galisteo, A.L. Sánchez, F.A. Williams, Systematically derived one-step kinetics for hydrogen-air gas-turbine combustion, *Combust. Flame* 250 (2023) 112633.

- [27] A.L. Sánchez, F.A. Williams, Recent advances in understanding of flammability characteristics of hydrogen, *Prog. Energ. Combust.* 41 (2014) 1-55.
- [28] S.A. Lloyd, F.J. Weinberg, A burner for mixtures of very low heat content, *Nature* 251 (1974) 47-49.
- [29] S.A. Lloyd, F.J. Weinberg, Limits to energy release and utilisation from chemical fuels, *Nature* 257 (1975) 367-370.
- [30] A.R. Jones, S.A. Lloyd, F.J. Weinberg, Combustion in heat exchangers, *P. R. Soc. Lond. A. Mat.* 360 (1978) 97-115.
- [31] P. Ronney, Analysis of non-adiabatic heat-recirculating combustors, *Combust. Flame* 135 (2003) 421-439.
- [32] Y. Ju, C.W. Choi, An analysis of sub-limit flame dynamics using opposite propagating flames in mesoscale channels, *Combust. Flame* 133 (2003) 483-493.
- [33] R.V. Fursenko, S. S. Minaev, Flame stability in a system with counter-flow heat exchange, *Combust. Explos. Shock+* 41 (2005) 133-139.
- [34] I. Schoegl, J.L. Ellzey, Superadiabatic combustion in conducting tubes and heat exchangers of finite length, *Combust. Flame* 151 (2007) 142-159.
- [35] J.A. Federici, D.G. Vlachos, A computational fluid dynamics study of propane/air microflame stability in a heat recirculation reactor, *Combust. Flame* 153 (2008) 258-269.
- [36] I.M. Schoegl, J.L. Ellzey, Numerical investigation of ultra-rich combustion in counter-flow heat exchangers, *Combust. Sci. Technol.* 182 (2010) 1413-1428.
- [37] V.N. Kurdyumov, M. Matalon, Analysis of an idealized heat-recirculating microcombustor, *Proc. Combust. Inst.* 33 (2011) 3275-3284.
- [38] M. Sánchez-Sanz, Premixed flame extinction in narrow channels with and without heat recirculation, *Combust. Flame* 159 (2012) 3158-3167.

- [39] E.L. Belmont, P. Radyjowski, J. L. Ellzey, Effect of geometric scale on heat recirculation and syngas production in a noncatalytic counter-flow reformer, *Combust. Sci. Technol.* 187 (2015) 874-893.
- [40] E. Fernández-Tarrazo, M. Sánchez-Sanz, R. Fursenko, S. Minaev, Multiple combustion regimes and performance of counter-flow microcombustor with power extraction, *Math. Model. Nat. Pheno.* 13 (2018) 52.
- [41] D. Fernández-Galisteo, E. Fernández-Tarrazo, C. Jiménez, V.N. Kurdyumov, Analysis of an idealized counter-current microchannel-based reactor to produce hydrogen-rich syngas from methanol, *Int. J. Hydr. Eng.* 44 (2019) 23807-23820.
- [42] V.N. Kurdyumov, D. Fernández-Galisteo, C. Jiménez, Superadiabatic small-scale combustor with counter-flow heat exchange: Flame structure and limits to narrow-channel approximation, *Combust. Flame* 222 (2020) 233-241.
- [43] A.C. Fernández-Pello, Micropower generation using combustion: issues and approaches, *Proc. Combust. Inst.* 29 (2002) 883-899.
- [44] D. Dunn-Rankin, E.M. Leal , D.C. Walther, Personal power systems, *Prog. Energ. Combust.* 31 (2005) 422-465.
- [45] Y. Ju, K. Maruta, Microscale combustion: technology development and fundamental research, *Prog. Energ. Combust.* 37 (2011) 669-715 .
- [46] D.C. Walther, J. Ahn, Advances and challenges in the development of power-generation systems at small scales, *Prog. Energ. Combust.* 37 (2011) 583-610 .
- [47] K. Maruta, Micro and mesoscale combustion, *Proc. Combust. Inst.* 33 (2011) 125-150.
- [48] N.S. Kaisare, D.G. Vlachos, A review on microcombustion: fundamentals, devices and applications, *Prog. Energ. Combust.* 38 (2012) 321-359.
- [49] J.L. Ellzey, E.L. Belmont, C.H. Smith, Heat recirculating reactors: Fundamental research and applications, *Prog. Energ. Combust.* 72 (2019) 32-58.

- [50] J. Bosch, D. Fernández-Galisteo, C. Jiménez, V.N. Kurdyumov, Analytical study of superadiabatic small-scale combustors with a two-step chain-branching chemistry model: lean burning below the flammability limit, *Combust. Flame* 235 (2022) 11173.
- [51] J. Bosch, D. Fernández-Galisteo, C. Jiménez, V.N. Kurdyumov, Superadiabatic small-scale combustors: Asymptotic analysis of a two-step chain-branching combustion model, *Proc. Combust. Inst.* (2023), <http://doi.org/10.1016/j.proci.2022.07.065>.
- [52] V.N. Kurdyumov, C. Jiménez, Flame stabilization in narrow channels by a highly conductive wall segment: Application to small-scale combustion devices, *Combust. Flame* 245 (2022) 112348.
- [53] V.N. Kurdyumov, Lewis number effect on the propagation of premixed flames in narrow adiabatic channels: Symmetric and non-symmetric flames and their linear stability analysis, *Combust. Flame* 158 (2011) 1307-1317.
- [54] V.N. Kurdyumov, C. Jiménez, Propagation of symmetric and non-symmetric premixed flames in narrow channels: Influence of conductive heat-losses, *Combust. Flame* 161 (2014) 927-936.

## Figure captions

**Figure 1.** Sketch of the problem, coordinate system and opposite-velocity profiles in two channels; the computational domain is marked with a dash-dotted line rectangle.

**Figure 2.** The flame position  $x_f$  in the rightward flowing channel versus the flow rate  $m$  plotted for  $q = 0.8$  (left plot),  $q = 0.5$  (right plot) and various  $a$ ; all curves calculated for  $\ell = 40$  and  $b = 0.15$ . Dashed lines show the asymptotic case  $h_w \rightarrow 0$ ; open circles mark the maximum values of the flow rate; filled circles (left plot) correspond to initial conditions for the simulations presented in Fig. 3. The marked segments correspond to non-symmetric solutions, of which an example is shown in Fig. 8.

**Figure 3.** Examples illustrating evolutions of the flame position,  $x_f$ , for  $\ell = 40$ ,  $q = 0.8$ ,  $b = 0.15$ ,  $a = 3$  in the rightward flow direction channel; the initial conditions correspond to the states lying above the turning point in Fig. 2 (marked with filled circles) for  $m = 2$  (initially symmetric state) and  $m = 1.71$  (initially non-symmetric state). Horizontal dashed lines mark the corresponding stable states.

**Figure 4.** Temperature contour plots illustrating the states corresponding to the points indicated with open squares in Fig. 2 (right) for  $q = 0.5$ .

**Figure 5.** Temperature contour plots illustrating the unstable state corresponding to the point indicated with open square in Fig. 2 (left).

**Figure 6.** The dependence of  $x_f$  on  $q$  calculated for  $m = 2$  and different values of the channel width  $a$ . Open circles mark the critical values of  $q$  below which combustion is impossible (for a given value of  $m$ ).

**Figure 7.** Temperature distributions along the channel axis, for different values of  $a$  calculated for  $m = 2$ ,  $q = 1.2$  (upper plot) and  $q = 0.5$  (right plot); the dimensionless heat of reaction corresponding to the flammability limit is  $q_f = 0.8827$  for  $\beta = 10$ ,  $\gamma = 0.7$  and  $Le_F = 1$ .

**Figure 8.** An example of the temperature distribution along the channel axis for a non-symmetric (unstable) solution, calculated for  $\ell = 40$ ,  $a = 5$ ,  $q = 0.8$  and  $m \approx 1.28$ .

**Figure 9.** The dependence of the position of the flame in the channel on the flow rate for various  $a$ , for  $b = 1$ ,  $\ell = 40$  and  $q = 5$ . The limiting  $a \rightarrow 0$  solutions are shown by a dashed line.

**Figure 10.** Flame position value obtained at different values of  $a$ , for  $\ell = 40$ ,  $q = 0.8$ ,  $m = 2$  and  $b = 0.15$ .

**Figure 11.** An example of temperature distribution in a device with a finite

wall thickness,  $h_w = 0.5$ , plotted for  $m = 3$ ,  $\ell = 20$ ,  $a = 3$ ,  $b = 2$  and  $q = 0.8$ . **Figure 12.** Examples of variable distributions along the channel axis calculated for  $h_w = 0.5$ , upper plot for  $q = 0.8$  and  $m = 3$ , lower plot for  $q = 0.5$  and  $m = 0.8$ .

**Figure 13.** Dependence of the flame position in the channel on the flow rate  $m$  calculated for  $q = 0.8$  and  $0.5$ , all curves calculated with  $\ell = 20$ ,  $a = 1$ ,  $b = 2$ ; solid line -  $h_w = 0.5$ , dotted line -  $h_w \rightarrow 0$ .

**Figure 14.** Dependence of the flame position on the value of the wall thickness, calculated for  $m = 3$ ,  $b = 2$ ,  $q = 0.8$  and  $\ell = 20$ . Dashed lines indicate the limiting values calculated in the limit  $h_w \rightarrow 0$ .

**Figure 16.** Dependence of the flammability limit critical value for the dimensionless heat of reaction on the Zel'dovich number, for  $\gamma = 0.7$  and  $Le_F = 1$ ; the solid line represents the solution of Eqs. (25) and (26), the lines with long and short dashes show one and two terms in the asymptotic expansion (27), respectively.